Plasmonics (2022) 17:1985–1997
https://doi.org/10.1007/s11468-022-01680-1

Optical Property Analysis of Chitosan-Graphene Quantum Dots Thin Film and Dopamine Using Surface Plasmon Resonance Spectroscopy

Faten Bashar Kamal Eddin[1] · Yap Wing Fen[1,2] · Amir Reza Sadrolhosseini[3] · Josephine Ying Chyi Liew[1] · Wan Mohd Ebtisyam Mustaqim Mohd Daniyal[2]

Received: 8 March 2022 / Accepted: 7 June 2022 / Published online: 27 June 2022

Abstract

In this study, surface plasmon resonance (SPR) technique has been utilized to characterize the optical properties of chitosan-graphene quantum dots (CS-GQDs) thin film and dopamine (DA). Theoretical fitting of SPR dips yielded refractive indices of DA solutions and CS-GQDs thin films, as well as the thickness of the thin film. For DA solution, n and k values were the same as deionized water for all concentrations. The values of n and k for CS-GQDs thin film were 1.6990 and 0.1302 respectively before contacting DA. The experimental SPR reflectance curves obtained using CS-GQDs thin film were shifted continuously to the right with increasing DA concentrations. After adsorption of DA molecules, both n and thickness of the CS-GQDs thin film increased, while the value of k decreased. This, in turns, enhanced the SPR sensitivity towards DA. The obtained results underscore the appropriate and sufficient potential of the used technique to measure refractive index variations in real-time when very low concentration was used (1 fM) with refractive index sensitivity of 10.186°/RIU.

Keywords Surface plasmon resonance · Optical characterization · Dopamine · Sensitivity enhancement · Graphene quantum dots · Refractive index sensing

Introduction

Optical properties of materials are an attractive object for researchers and describe the response of the material when it interacts with light. The measurements of the optical properties of materials require a high degree of accuracy and precision for the advancement of optical technology. They have made a change in the life of the whole world in the field of medicine, sensors, astronomy, manufacturing, communication, etc. Such measurements include reflectance, transmittance, emittance, absorptance, and index of refraction [1]. Any of these quantities depends on geometry and polarization. Refractive index is a fundamental optical property of the material [2–4]. Refractive index of the medium is dependent on its chemical composition, and significantly can be influenced by temperature [5, 6]. It plays a pivotal role in light propagation in the medium and its reflection at an interface. This dimensionless constant is directly related to measurable quantities such as reflectance and absorption and defined as the ratio of the light speed in a vacuum to light phase velocity in the material. Among all the methods that were used to measure the refractive index, surface plasmon resonance (SPR) technique emerged and proved its efficiency in determining the refractive index value and detecting its local small changes in real time [7–16]. This is because the working principle of the SPR technique relies on the variation of the refractive index in the evanescent field at the sensing medium [17–23]. SPR as a refractive index–based sensing technique has attracted extensive attention over the past years due to its advantages of simplicity, cost effectiveness, and real-time and label-free detection [24–34]. These important advantages of SPR technology make it desirable for medical applications [35–55], control and safety of food [56, 57], environmental protection [58–74], and other

✉ Yap Wing Fen
yapwingfen@upm.edu.my

[1] Department of Physics, Faculty of Science, Universiti Putra Malaysia (UPM), 43400 UPM Serdang, Selangor, Malaysia

[2] Functional Nanotechnology Devices Laboratory, Institute of Nanoscience and Nanotechnology, Universiti Putra Malaysia (UPM), 43400 UPM Serdang, Selangor, Malaysia

[3] Magneto-Plasmonic Lab, Laser and Plasma Research Institute, Shahid Beheshti University, Tehran 1983969411, Iran

uses. The refractive index is affected by the accumulation of mass on the surface of the metallic thin layer. The adsorption of target molecules on the thin film induces the variation of the refractive index. The changes in the thin film optical properties shift the SPR dip, such that the SPR angular shifts and the refractive index variation could be measured. Also, the concentration changes could be detected and the binding affinity could be determined [75]. In this study, dopamine, the important neurotransmitter that controls the functions of the human body, will be the detected target and its refractive index will be determined. This will be conducted using the gold thin film only first. To ensure the adsorption efficiency of DA molecules and to improve the thin film sensitivity to the variations in refractive index, the gold thin film has to be modified using nanomaterials. In recent years, graphene quantum dots (GQDs) have captured the interest due to their distinctive photoluminescence properties, remarkable physicochemical properties, good photostability, biocompatibility, and low toxicity [76–80]. The incorporation of GQDs with chitosan (CS) the biopolymer with many amine groups will increase DA adsorption on the thin film [48]. To the best of our knowledge, the utilization of SPR technique to study CS-GQDs thin film optical properties and determine its thickness before and after interaction with DA has not been conducted yet.

Materials and Methods

Preparation of Chemicals

Dopamine hydrochloride, GQDs (1 mg/ml), CS and acetic acid (assay ≥ 99.7%) were purchased from Sigma-Aldrich. Firstly, 200 mg of chitosan was taken and dissolved in 25 ml of 1% acetic acid, stirred and left at room temperature overnight to obtain a homogeneous CS solution [29]. After that, 2 ml of pure GQDs was added into 10 ml of CS solution with stirring to form CS-GQDs solution. Then, deionized water (DW) was utilized to dilute 1 M solution of DA to get very low levels down to 1 fM using the dilution formula ($M_1V_1 = M_2V_2$).

Preparation of Thin Films

The gold thin films were deposited on clean glass substrates of dimensions (24 mm × 24 mm × 0.1 mm) using SC7640 Sputter Coater. Then, the surface of gold thin layer on the glass substrate was uniformly covered by 0.5 ml of CS-GQDs mixture. And CS-GQDs thin films were deposited using spin coating technique at 2000 rpm during 30 s.

SPR Setup

To characterize the optical properties of the used solution and thin films, a custom-built SPR spectroscopy in Kretschmann configuration has been used. This homemade setup as shown in Fig. 1 contains a He–Ne laser at the wavelength (632.8 nm), a light chopper, a linear polarizer, a small pinhole, a prism (refractive index 1.77861), an optical rotating stage, a photodetector, and lock-in amplifier. SPR experiments were carried out for the gold thin film and CS-GQDs thin film that contact deionized water and DA with different concentrations. To record the reference signal, deionized water was inserted into the flow cell to be in contact with the gold thin film and then with the sensing layer one by one. After that, various levels of DA solution ranging from 1 to 1000 fM were inserted separately into the flow cell one after one to carry out the measurements by recording the intensity of the reflected laser light as a function of the incident angle.

Fitting of Experimental Results to Theoretical

When plasmonic resonance occurs, and the partial transfer of the pumping light energy to the electron packages on the metal film takes place, surface plasmon wave with a transversally magnetic (TM) mode propagates freely along the metal thin film-dielectric interface. Its propagation depends strongly on the real and imaginary parts of the dielectric constants of these two media. The electric field component, E, is parallel to the incidence plane and perpendicular to the metal–dielectric interface while the magnetic field component, B, is perpendicular to incidence plane and lies in the plane of metal–dielectric interface [81]. Fresnel theory was used to investigate the interaction of the light and surface plasmons. In this work, the gold thin film and the sensor layer (CS-GQDs thin film) were sandwiched between the prism and the dielectric medium (DA solution) in Kretschmann configuration.

The magnitudes of the magnetic field and the electric field are related as shown in the following expression [82] :

$$B = \frac{E}{V} \tag{1}$$

where V is the wave speed and related to the speed of light in a vacuum c and the refractive index n by:

$$V = \frac{c}{n} \tag{2}$$

The constant c can be written as:

$$c = \frac{1}{\sqrt{\varepsilon_0 \mu_0}} \tag{3}$$

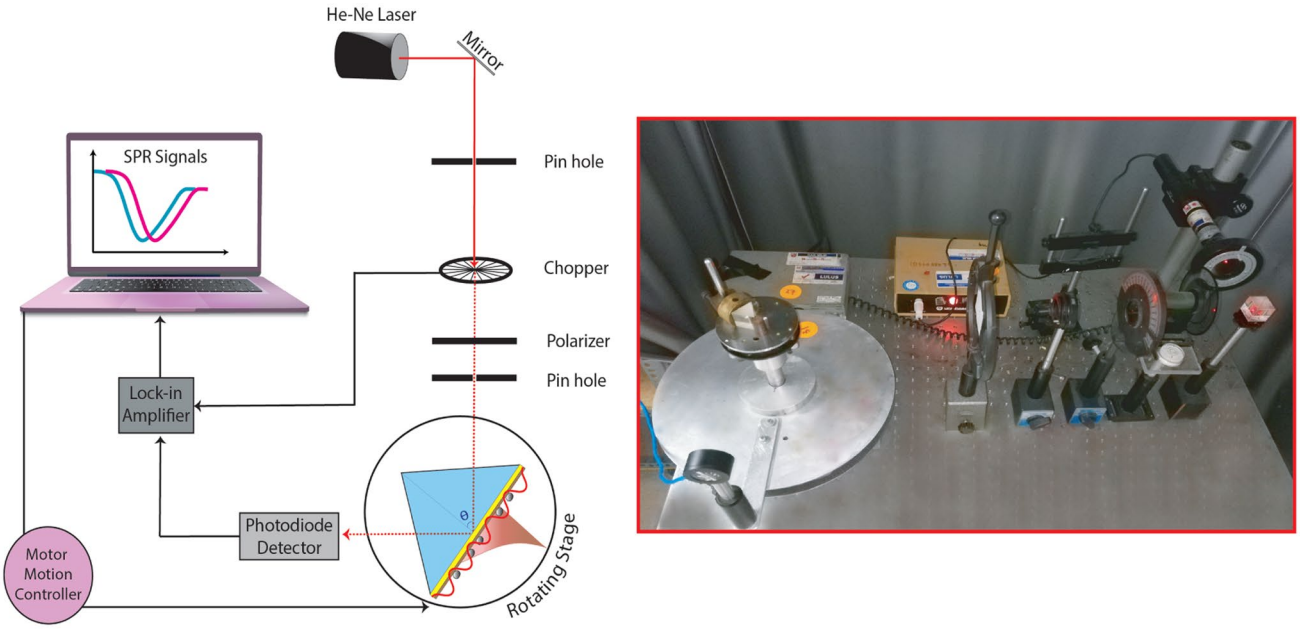

Fig. 1 SPR setup

where ε_0 and μ_0 are the permittivity and permeability of free space, respectively.

By combining Eqs. (1), (2), and (3), the magnitude of B can be written as:

$$B = \frac{E}{V} = \frac{n}{c}E = n\sqrt{\varepsilon_0\mu_0}E \tag{4}$$

By using Eq. (4) and based on Fig. 2 where the boundary conditions are satisfied at the both interfaces, the magnetic and electric fields are related as follows:

$$B_a = n_0\sqrt{\varepsilon_0\mu_0}\left(E_0 + E_{r1}\right) = n_1\sqrt{\varepsilon_0\mu_0}\left(E_{t1} + E_{i1}\right) \tag{5}$$

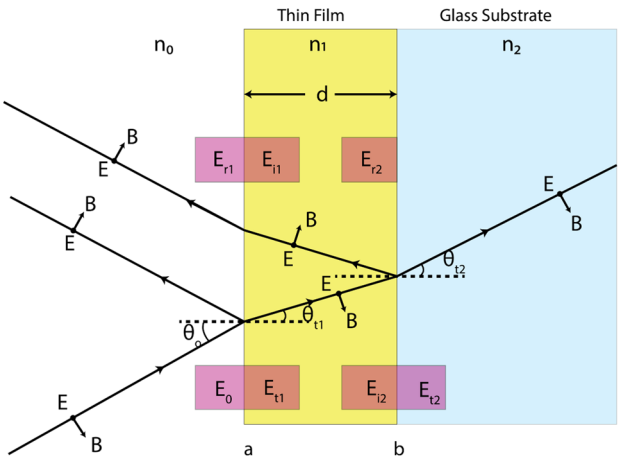

Fig. 2 Light reflection from a single layer with thickness d [84]

$$B_b = n_1\sqrt{\varepsilon_0\mu_0}\left(E_{i2} + E_{r2}\right) = n_2\sqrt{\varepsilon_0\mu_0}E_{t1} \tag{6}$$

$$E_a = \left(E_0 - E_{r1}\right)\cos\left(\theta_0\right) = \left(E_{t1} - E_{i1}\right)\cos\left(\theta_{t1}\right) \tag{7}$$

$$E_b = \left(E_{i2} - E_{r2}\right)\cos\left(\theta_{t1}\right) = E_{t2}\cos\left(\theta_{t2}\right) \tag{8}$$

where E_{rl} denotes the sum of all the multiple reflected beams from the thin film at the interface (a) as shown in Fig. 2, while E_{i2} denoted the sum of all the multiple beams incident on the glass substrate at the interface (b), and so on.

When different layers are used, after light passes through them the phase changes. Taking this into consideration gives:

$$E_{i1} = E_{r2}e^{-i\delta}, E_{i2} = E_{t1}e^{-i\delta} B_{i1} = B_{r2}e^{-i\delta}, B_{i2} = B_{t1}e^{-i\delta} \tag{9}$$

The relationships between E_1, B_1 and E_2, B_2 can be obtained as follows using Euler identities:

$$E_a = \cos(\delta)E_b - \frac{i\sin(\delta)}{\gamma_1}B_b \tag{10}$$

$$B_a = -\gamma_1 i\sin\left(\delta\right)E_b + \cos(\delta)B_b \tag{11}$$

$$\text{where } \gamma_1 = \frac{n_1}{\cos\left(\theta_{t1}\right)}\sqrt{\varepsilon_0\mu_0} \tag{12}$$

Equations (10) and (11) can be combined in matrix form as:

$$\begin{bmatrix} E_a \\ B_a \end{bmatrix} = \begin{bmatrix} \cos(\delta) & -\frac{i\sin(\delta)}{\gamma_1} \\ -\gamma_1 i \sin(\delta) & \cos(\delta) \end{bmatrix} \begin{bmatrix} E_b \\ B_b \end{bmatrix} \tag{13}$$

Thus, in the case of single layer with thickness d, the transfer matrix will be as follows:

$$M_1 = \begin{bmatrix} \cos(\delta) & -\frac{i\sin(\delta)}{\gamma_1} \\ -\gamma_1 i \sin(\delta) & \cos(\delta) \end{bmatrix} \tag{14}$$

where δ represents the phase shift when the light passes through multilayers:

$$\delta = \frac{2\pi}{\lambda} d\, n_1 \cos(\theta_{t1}) \tag{15}$$

When different layers are used, the glass substrate at boundary b will be replaced by the interface of the thin film added. In this case, Eq. (13) is still valid but second transfer matrix is needed to relate E_b and B_b to E_c and B_c at the rear boundary of the second thin film. Thus, for a multilayer film with N number of layers,

$$\begin{bmatrix} E_a \\ B_a \end{bmatrix} = \prod_{i=1}^{N} M_N \begin{bmatrix} E_N \\ B_N \end{bmatrix} \tag{16}$$

For the entire multilayer films, the inclusive transfer matrix M_T can be represented by:

$$M_T = \begin{bmatrix} m_{11} & m_{21} \\ m_{12} & m_{22} \end{bmatrix} \tag{17}$$

where m_{11}, m_{12}, m_{21}, and m_{22} denote the elements of the transfer matrix.

Using Eqs. (5), (6), (7), (8), and (16), we get

$$\begin{bmatrix} (E_0 - E_{r1})\cos(\theta_0) \\ n_0\sqrt{\varepsilon_0\mu_0}(E_0 + E_{r1}) \end{bmatrix} = \begin{bmatrix} m_{11} & m_{21} \\ m_{12} & m_{22} \end{bmatrix} \begin{bmatrix} E_{t2}\cos(\theta_{t2}) \\ n_2\sqrt{\varepsilon_0\mu_0}E_{t1} \end{bmatrix} \tag{18}$$

By simplifying the previous equations and using the reflection coefficient r that defined as

$$r = \frac{E_{r1}}{E_0} \tag{19}$$

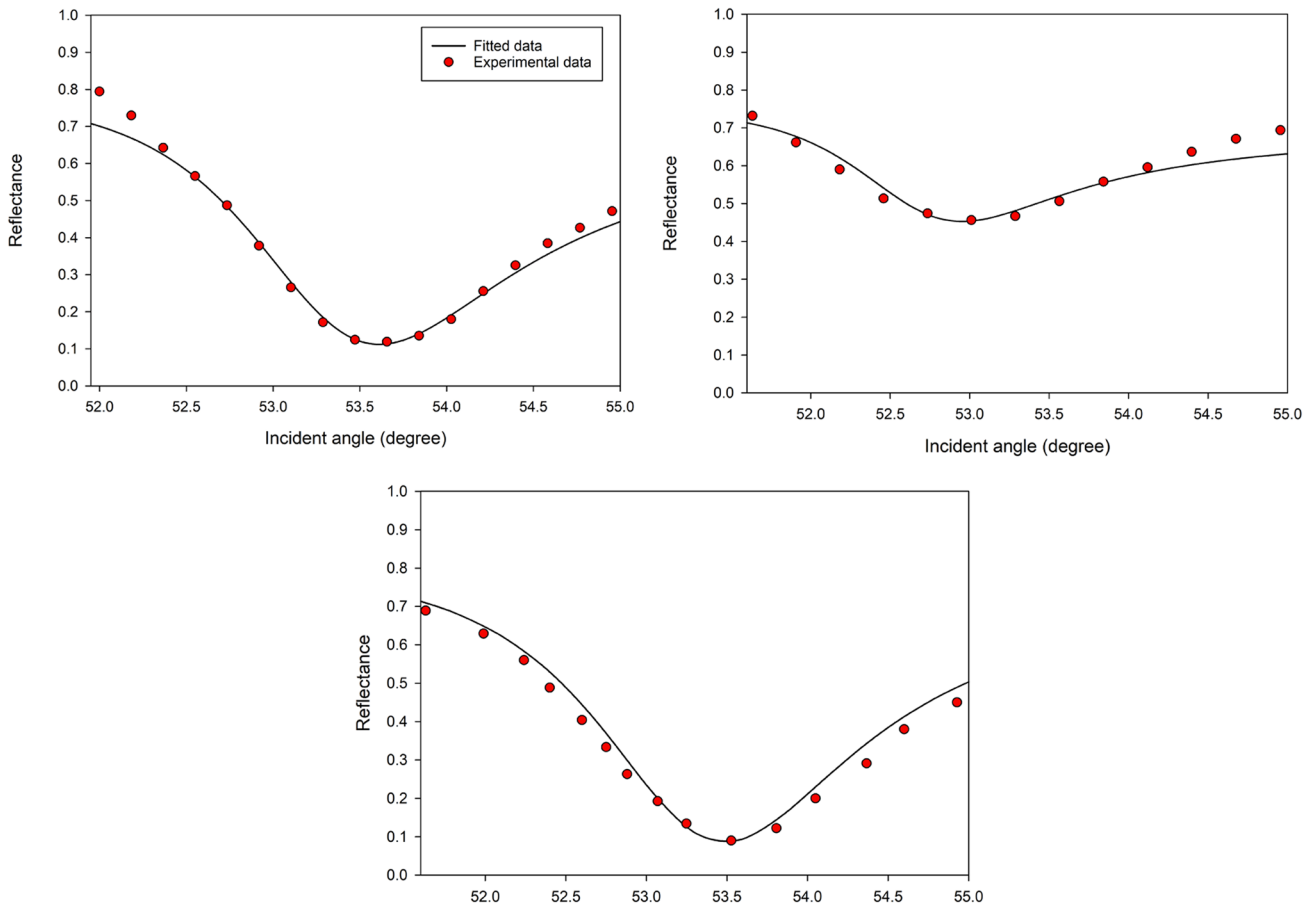

Fig. 3 Fitted reflectance curves of three gold thin films exposed to DW

Table 1 Refractive index and thickness of the gold thin films exposed to DA

Gold layer	Refractive index of Au layer		Thickness d (nm) (± 0.01)
	Real part, n (± 0.0001)	Imaginary part, k (± 0.0001)	
1	0.2164	3.6867	53.67
2	0.2758	3.8798	63.26
3	0.1205	3.6920	59.40

the reflection coefficient will be written in the following formula

$$r = \frac{m_{21} + m_{22}\gamma_2 - m_{11}\gamma_0 - m_{12}\gamma_2\gamma_0}{m_{21} + m_{22}\gamma_2 + m_{11}\gamma_0 + m_{12}\gamma_2\gamma_0} \quad (20)$$

whereby the reflectivity R is

$$R = rr^* \quad (21)$$

All reflectance curves obtained using the gold thin films were analyzed using a developed fitting program based on the equations explained above to evaluate the optical properties and the thickness of the gold thin film as well as the optical properties of DA solution. This information then was used for a subsequent mathematical processing and analyzing of the optical properties and thickness of CS-GQDs thin film before and after interaction with DA solution of different concentrations based on the mentioned matrix method [83–87].

Results and Discussion

Characterization the Optical Properties of Gold Thin Film

At the first stage, the prefatory SPR experiment was conducted for gold thin films in contact with DW in order to determine the optical properties of the gold thin layer (the real and imaginary parts of refractive index, n and k respectively; in addition to the thickness of the thin film, d). The optical properties of the three gold layers used were obtained by fitting the reflectance curve as shown in Fig. 3. According to the fitted SPR signal, the refractive index values, n and k, for the first gold thin layer were (0.2164 ± 0.0001) and (3.6867 ± 0.0001) respectively, where the thickness, d, was determined as (53.67 ± 0.01) nm. The refractive index for DW water in room temperature is 1.3333 [88]. The optical properties of the other gold thin films used are listed in Table 1.

Characterization of DA Optical Properties

The SPR experiments were also conducted for all concentrations (ranging from 1 to 1000 fM) of DA solutions contacting the second gold thin film to determine the refractive index of the solutions. The experimental SPR curves were not shifted from the reference curve with increasing the DA level as shown in Fig. 4. These experimental curves were fitted with theoretical data for gold thin film in contact with DA solutions as shown in Fig. 5. Using the obtained

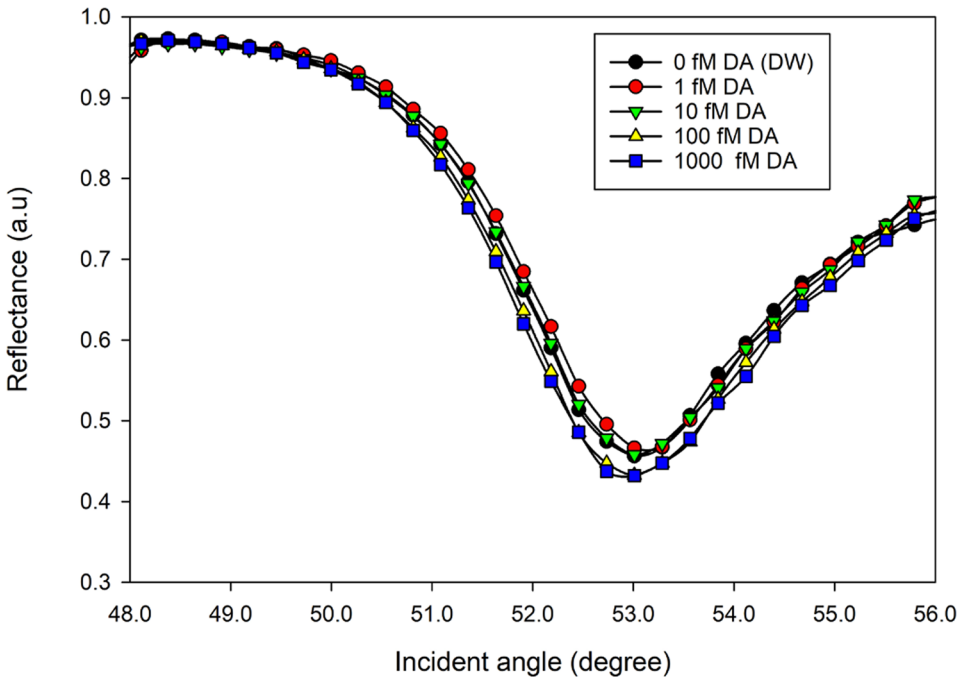

Fig. 4 The experimental SPR curves of the gold thin film exposed to different levels of DA

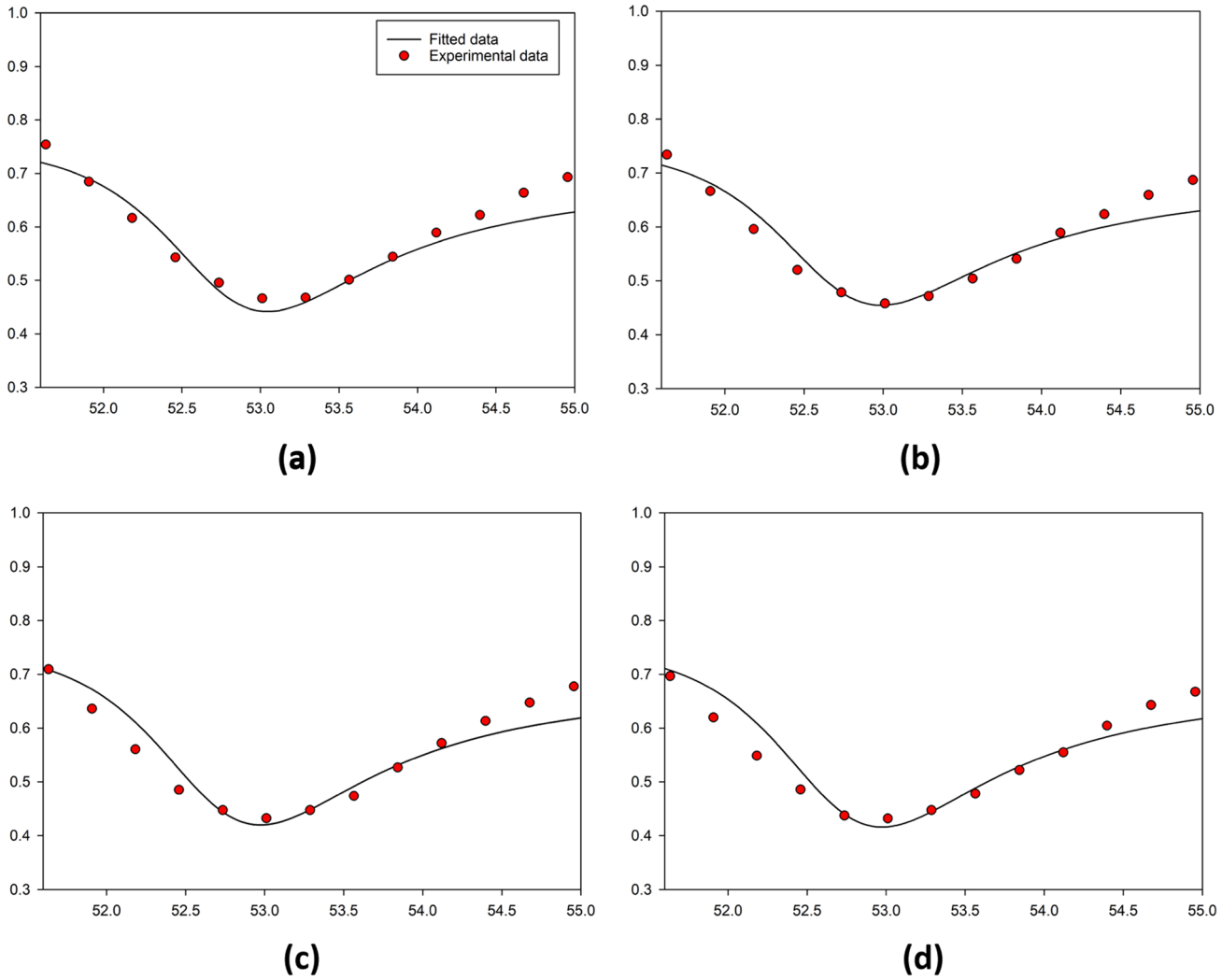

Fig. 5 Experimental and fitted reflectance curves related to the gold thin film exposed to DA solution for **a** 1 fM, **b** 10 fM, **c** 100 fM, and **d** 1000fM

thickness and refractive index of the second gold layer *d* (63.26) nm, *n* (0.2758), and *k* (3.8798), the fitting yielded the real part, *n*, and imaginary part, *k*, of DA solutions which were the same as the refractive index of DW as illustrated in Table 2. Also, the *n, k,* and *d* values of the bare gold film were not changed with increasing DA levels. These findings ($\Delta\theta = 0$, and $\Delta n = 0$) confirmed that the adsorption of DA molecules on the film surface did not take place, and demonstrated the insensitivity of Au-based sensor towards DA. The dependence of the complex index of refraction on the concentration at room temperature was not obvious for the used concentrations of DA transparent solution. Here, because the analyte concentrations are sufficiently low (1 fM to 1000 fM), the refractive index remained constant [89].

Table 2 Refractive index of both the gold film and DA solution after contact

DA concentration (fM)	Refractive index of gold film		Refractive index of DA solution	
	Real part, *n* (±0.0001)	Imaginary part, *k* (±0.0001)	Real part, *n* (±0.0001)	Imaginary part, *k* (±0.0001)
0	0.2758	3.8798	1.3333	0.0000
1	0.2758	3.8798	1.3333	0.0000
10	0.2758	3.8798	1.3333	0.0000
100	0.2758	3.8798	1.3333	0.0000
1000	0.2758	3.8798	1.3333	0.0000

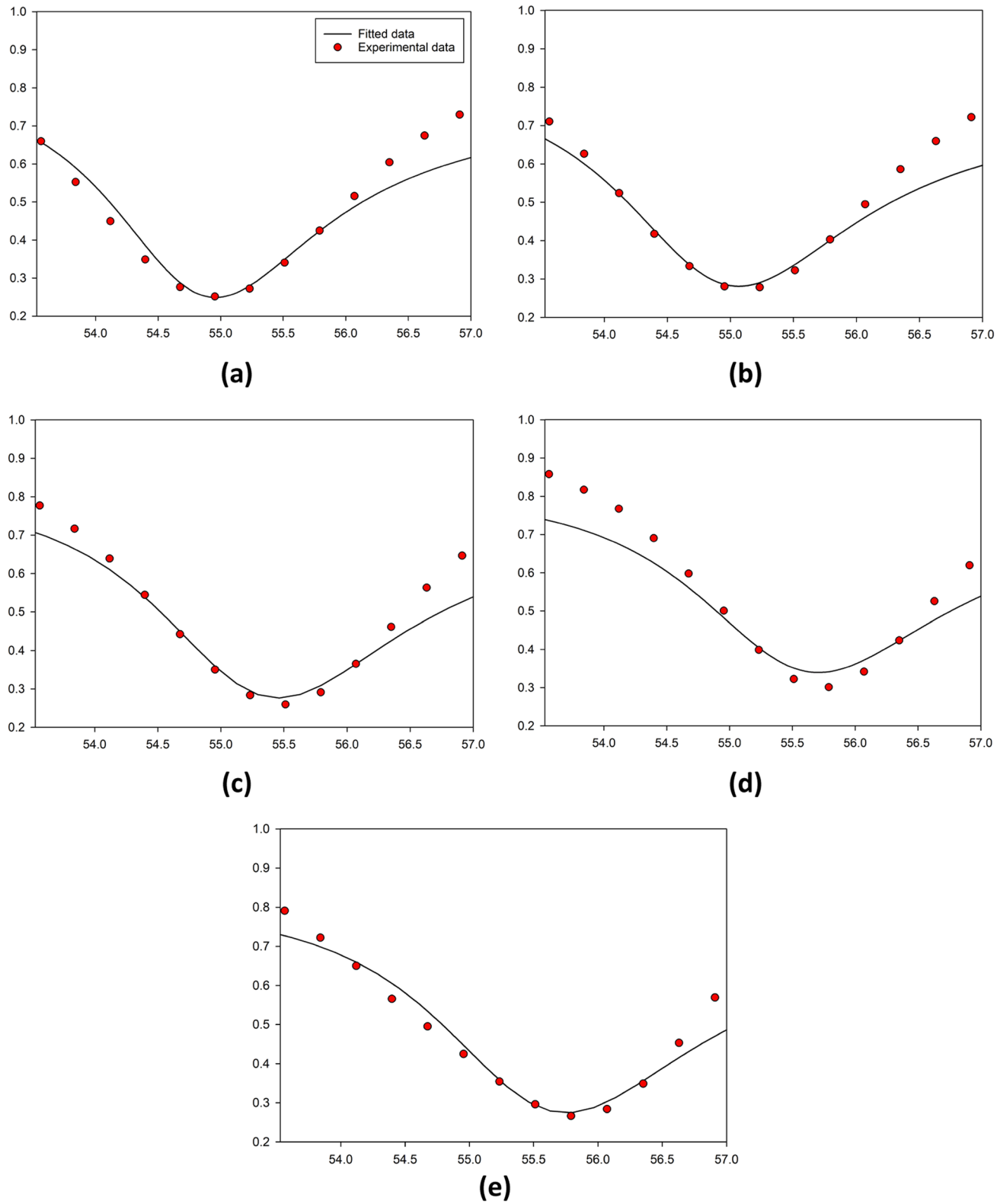

Fig. 6 The experimental and fitted reflectance curves of the CS-GQDs thin layer exposed to DA solution for **a** 0 fM, **b** 1 fM, **c** 10 fM, **d** 100 fM, and **e** 1000 fM

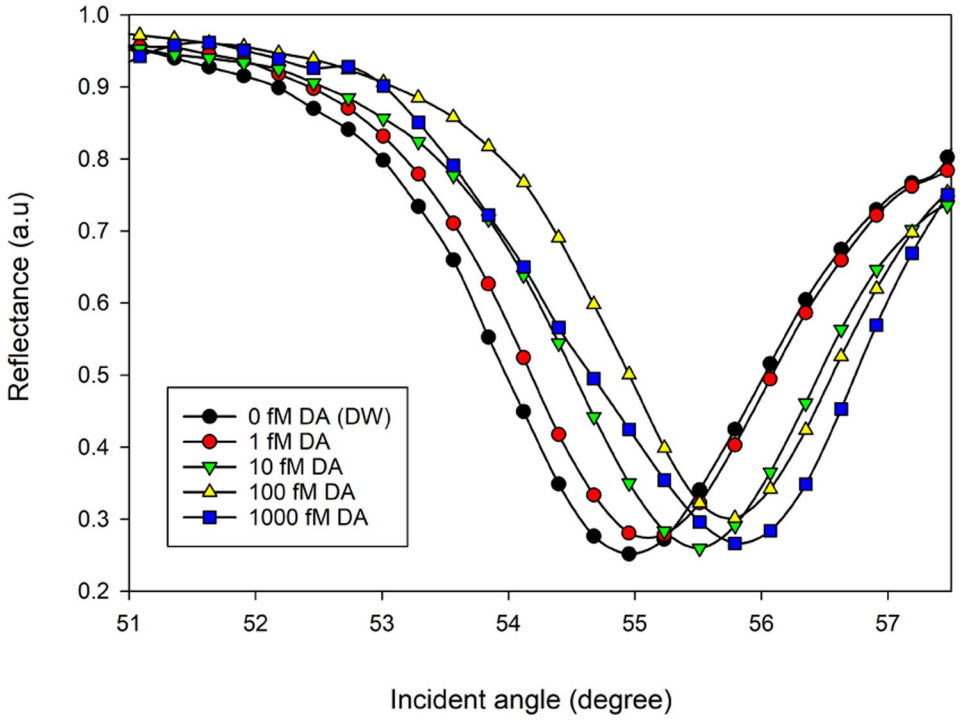

Fig. 7 The experimental SPR curves of the CS-GQDs thin film exposed to different levels of DA

Characterization of CS-GQDs Optical Properties

To investigate and determine the optical properties of the CS-GQDs thin film, the prepared thin film was placed on one of the sides of the prism in the SPR spectroscopy. Above all, the SPR measurement was conducted by injecting deionized water into the flow cell to contact the CS-GQDs thin film. After recording the reflected beam, the results showed that when this sensing layer was used and contacted the DW, the plasmonic resonance occurred at higher angle compared with the case of the gold thin film, and the SPR dip was shifted significantly to the right. This is due to the difference in refractive index value and the thickness of the CS-GQDs thin film compared to the third gold thin film used. The refractive index values for both gold thin film and DA solution as well as the thickness of the gold thin film obtained were used to analyze the optical properties of the CS-GQDs thin film. After fitting the experimental reflectance curve using the obtained refractive index and thickness of the third gold layer n (0.1205), k (3.6920), and d (59.4) nm as shown in Fig. 6, the values of refractive index, n and k, for the sensing layer were (1.6990 ± 0.0001) and (0.1302 ± 0.0001) respectively, where the thickness, d, was determined (6.36 ± 0.01) nm. After that, the SPR experiment was continued with DA solutions. The inserted sample of DA into the system with concentration of 1 fM led to increase the resonance angle and shifted the SPR dip to the right remarkably as shown in Fig. 7. Continuing to gradually increase the concentration of DA up to 1000 fM gave the opportunity for more DA molecules to attach to the surface of CS-GQDS thin film and change its optical properties, and all this, in turn, led to more angular shift of the SPR signals to the right. The fitting showed that the real part n of the refractive index of CS-GQDs has increased from 1.6990 to 1.6999 and the thickness became 7.26 nm. The results showed

Table 3 The real and imaginary parts of refractive index and the thickness of CS-GQDs thin film, $\Delta\theta$, and Δn, for different levels of DA solutions

DA concentration (fM)	Refractive index of CS-GQDs layer exposed to DA		Thickness of CS-GQDs layer d (nm) (± 0.01)	Δn	$\Delta\theta$
	Real part, n (± 0.0001)	Imaginary part, k (± 0.0001)			
0	1.6990	0.1302	6.36	0.0000	0.00000
1	1.6999	0.1301	7.26	0.0009	0.27831
10	1.7590	0.1300	7.60	0.0600	0.55855
100	1.7750	0.1290	8.61	0.0760	0.83678
1000	1.7820	0.1140	8.64	0.0830	0.83734

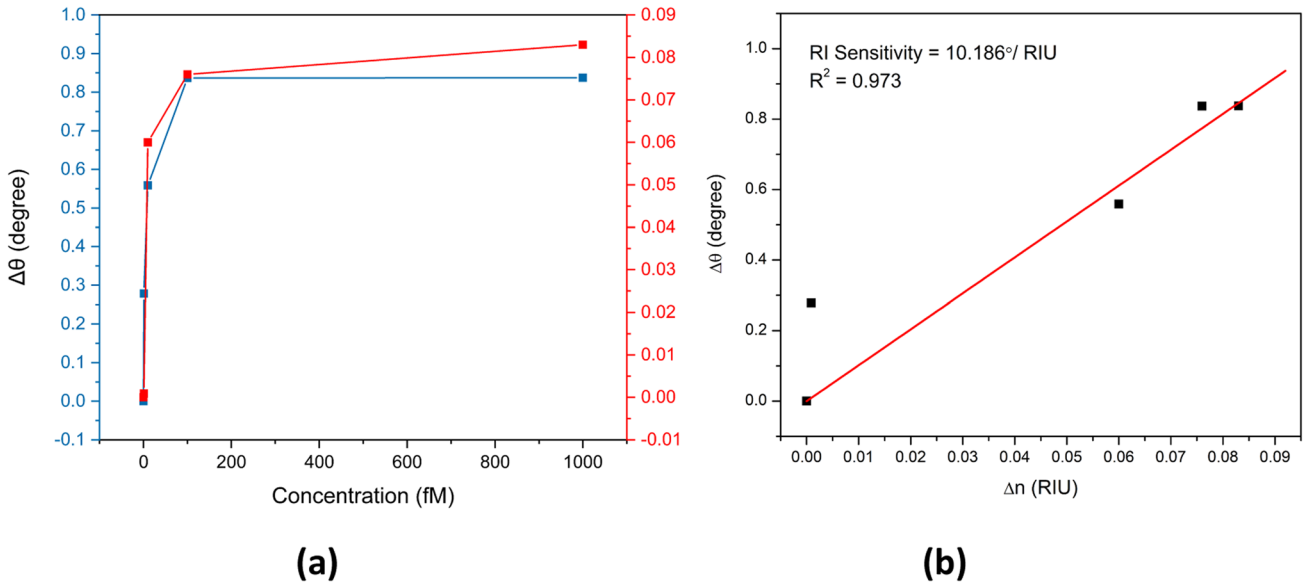

Fig. 8 **a** The variation of $\Delta\theta$ and Δn with DA concentrations, and **b** the refractive index sensitivity of the CS-GQDs thin film for DA sensing

that the values of n of the sensing layer CS-GQDs increased from 1.6990 to 1.7820 as the level of DA solutions increased from 0 to 1000 fM, while the k values decreased from 0.1302 to 0.1140. The thickness of the proposed active layer increased from 6.36 to 8.64 nm using this range of DA concentrations as shown in Table 3. These changes in the values of the refractive index and the enhancement of the sensor sensitivity towards DA might be due to the electrostatic interactions, hydrogen bonding, and strong π-π interaction of DA with the functional groups of the GQDs, and what reinforced this interaction is the electrostatic attraction between CS and DA [77, 90]. During these interactions, more molecules of DA were captured on the CS-GQDs thin layer and led to changes in its refractive index and thickness. This, in turn, shifted the SPR dips significantly to the right because the SPR signal is very sensitive towards any change in the surrounding thin films.

Refractive Index Sensitivity of the SPR/CS-GQDs System

It is very important to evaluate the sensitivity of the utilized SPR technique. The refractive index sensitivity is defined as the ratio between the change of resonance angle, $\Delta\theta$, and the variation of the real part refractive index, Δn [91–95] :

$$S = \Delta\theta/\Delta n \tag{22}$$

The $\Delta\theta$ was calculated as the difference between the resonance angle of different concentrations of DA solution contacted CS-GQDs thin layer and the resonance angle of DW as shown in Table 3. The variation of real part refractive index, Δn, was calculated for CS-GQDs thin film that was exposed to all concentrations of DA. It is clear from Fig. 8(a) that both $\Delta\theta$ and Δn Increased gradually as a level of DA solution increased. This is because the binding of DA with different levels (0 to 1000 fM) to the surface of CS-GQDs thin film changed the refractive index of the film and this caused shifting of the SPR signals. As shown from Fig. 8(b), slope sensitivity of 10.186°/RIU (refractive index unit) was observed with a correlation coefficient, R^2 of 0.973. These results demonstrated the high potential and efficiency of SPR technique to monitor the changes in refractive index of CS-GQDs thin film when it contacts 1 fM of DA.

Conclusion

In the present study, SPR technique has been successfully developed and used to characterize the optical properties of DA solutions, gold thin films, and CS-GQDs thin films by theoretical fitting of the experimental SPR signals. The real part of the refractive index, n, and the imaginary part of the refractive index, k, for all gold thin films used were good as in agreement with the previous studies. The n and k values of DA solution for all concentrations were the same as deionized water. The values of n of the sensing layer CS-GQDs increased from 1.6990 to 1.7820 as the concentration of DA solutions increased, while the k values decreased from 0.1302 to 0.1140. The thickness of the proposed sensing layer increased from 6.36 nm to 8.64 nm. The results showed that the CS-GQDs thin layer has improved the sensitivity of the SPR sensor towards DA and the achieved sensitivity was 10.186°/RIU.

Acknowledgements F.B.K.E. acknowledges the support received from OWSD and Sida (Swedish International Development Cooperation Agency), the laboratory facilities provided by the Institute of Advanced Technology, Department of Physics, Department of Chemistry, Universiti Putra Malaysia.

Author Contribution Conceptualization, Y.W.F. and F.B.K.E.; methodology, writing—original draft preparation, F.B.K.E.; supervision, validation, funding acquisition, Y.W.F.; writing—review and editing, Y.W.F. and F.B.K.E.; resources, Y.W.F., J.Y.C.L., and W.M.E.M.M.D.; software, Y.W.F., A.R.S., F.B.K.E., and W.M.E.M.M.D.; visualization, F.B.K.E. All authors have read and agreed to the published version of the manuscript.

Funding This research was funded by the Ministry of Education Malaysia through the Fundamental FRGS (FRGS/1/2019/STG02/UPM/02/1) and Universiti Putra Malaysia through Putra Grant (GP-IPB/2021/9700700).

Data Availability Data sharing is not applicable to this article as no datasets were generated or analyzed during the current study.

Declarations

Ethics Approval Not applicable.

Consent to Participate Not applicable.

Consent for Publication Not applicable.

Conflict of Interest The authors declare no competing interests.

References

1. Javaheri S, Babaeipour M, Boochani A, Naderi S (2018) Electronic and optical properties of V doped A1N nanosheet : DFT calculations, Chinese. J Phys 56:2698–2709. https://doi.org/10.1016/j.cjph.2018.10.021
2. Singh S (2002) Refractive index measurement and its applications. Phys Scr 65:167–180. https://doi.org/10.1238/Physica.Regular.065a00167
3. Mistrik J, Kasap S, Ruda H, Koughia C (2017) Optical properties of electronic materials: fundamentals and characterization. In: Springer Handbook of Electronic and Photonic Materials. Springer, Cham. https://doi.org/10.1007/978-3-319-48933-9
4. Yang R, Shi M, Wei Q, Wu F, Xue M, Zhou Y (2019) A first-principles study of the properties of P-43m-$Si_{3\times2}$ (X=N, P and As), Chinese. J Phys 59:535–545. https://doi.org/10.1016/j.cjph.2019.04.007
5. Ibrahim J, Al Masri M, Verrier I, Kampfe T, Veillas C, Celle F, Cioulachtjian S, Lefèvre F, Jourlin Y (2019) Surface plasmon resonance based temperature sensors in liquid environment. Sensors 19:1–10. https://doi.org/10.3390/s19153354
6. Addanki S, Amiri IS, Yupapin P (2018) Review of optical fibers-introduction and applications in fiber lasers. Results Phys 10:743–750. https://doi.org/10.1016/j.rinp.2018.07.028
7. Phillips KS, Cheng QJ (2008) Surface plasmon resonance. https://doi.org/10.1007/978-1-60327-375-6_46
8. Wang Y, Knoll W, Dostalek J (2012) Bacterial pathogen surface plasmon resonance biosensor advanced by long range surface plasmons and magnetic nanoparticle assays. Anal Chem 84:8345–8350. https://doi.org/10.1021/ac301904x
9. Hong LH, Yahaya A, Munajat Y (2015) Simulation of surface plasmon resonance sensor. AIP Conf Proc 1674:1–6. https://doi.org/10.1063/1.4928832
10. Yanase Y, Sakamoto K, Kobayashi K, Hide M (2016) Diagnosis of immediate-type allergy using surface plasmon resonance. Opt Mater Express 6:1339. https://doi.org/10.1364/OME.6.001339
11. Mukhtar WM, Murat NF, Samsuri ND, Dasuki KA (2018) Maximizing the response of SPR signal: a vital role of light excitation wavelength. AIP Conf Proc 2016. https://doi.org/10.1063/1.5055506
12. Xia G, Zhou C, Jin S, Huang C, Xing J, Liu Z (2019) Sensitivity enhancement of two-dimensional materials based on genetic optimization in surface plasmon resonance. Sensors (Switzerland) 19. https://doi.org/10.3390/s19051198
13. Sadafi MM, Karami H, Hosseini M (2021) A tunable hybrid graphene-metal metamaterial absorber for sensing in the THz regime. Curr Appl Phys 31:132–140. https://doi.org/10.1016/j.cap.2021.07.020
14. SalmanOgli A, Nasseri B, Kohneh Shahri MY, Piskin E (2016) Plasmon – plasmon interaction effect on effective medium electrical conductivity (an effective agent for photothermal therapy). Curr Appl Phys 16:1498–1505. https://doi.org/10.1016/j.cap.2016.08.021
15. Gomaa M, Salah A, Abdel Fattah G (2022) Utilizing dip-coated graphene/nanogold to enhance SPR-based fiber optic sensor. Appl Phys A Mater Sci Process 128:1–12. https://doi.org/10.1007/s00339-021-05196-z
16. Kumar R, Pal S, Pal N, Mishra V, Prajapati YK (2021) High-performance bimetallic surface plasmon resonance biochemical sensor using a black phosphorus–MXene hybrid structure. Appl Phys A Mater Sci Process 127:1–12. https://doi.org/10.1007/s00339-021-04408-w
17. Wong CL, Olivo M (2014) Surface plasmon resonance imaging sensors : a review. 809–824. https://doi.org/10.1007/s11468-013-9662-3
18. Lei J, Ji B, Lin J (2016) A high-performance light absorber based on a metamaterial nanopyramid array, Chinese. J Phys 54:940–946. https://doi.org/10.1016/j.cjph.2016.09.003
19. Naz G, Butt FK, Bajwa SZ, Khan WS, Irfan M, Irfan M (2019) Au / Cu 2 O core / shell nanostructures with efficient photoresponses, Chinese. J Phys 59:307–316. https://doi.org/10.1016/j.cjph.2019.03.008
20. Ben H, Hocini A, Temmar MN, Khedrouche D (2019) Design of mid infrared high sensitive metal-insulator-metal plasmonic sensor, Chinese. J Phys 61:86–97. https://doi.org/10.1016/j.cjph.2019.07.006
21. Zhijian L, Qing Z, Yaonan W, Suxia X (2019) Fano resonance in asymmetric gold nano-dimers with square and rectangular sections, Chinese. J Phys 59:40–48. https://doi.org/10.1016/j.cjph.2019.01.018
22. Jiang Q, Boyu J, Peng L, Xiaowei S, Haiyan T, Yinping D, Xun G, Zuoqiang H, Jingquan L (2018) Investigation of ultrafast plasmon control in silver block by PEEM, Chinese. J Phys 56:340–345. https://doi.org/10.1016/j.cjph.2017.11.015
23. Pan M, Lee K, Wang L, Wei P (2017) Biosensors and bioelectronics chip-based digital surface plasmon resonance sensing platform for ultrasensitive biomolecular detection. Biosens Bioelectron 91:580–587. https://doi.org/10.1016/j.bios.2017.01.003
24. Caucheteur C, Guo T, Albert J (2015) Review of plasmonic fiber optic biochemical sensors : improving the limit of detection. Anal Bioanal Chem 3883–3897. https://doi.org/10.1007/s00216-014-8411-6
25. Huang Y, Wu D, Chuang C, Nie B, Cui H, Yun W (2015) Theoretical analysis of tapered fiber optic surface plasmon resonance sensor for voltage sensitivity. Opt Fiber Technol 22:42–45. https://doi.org/10.1016/j.yofte.2015.01.004

26. Arghir I, Spasic D, Verlinden BE, Delport F, Lammertyn J (2015) Improved surface plasmon resonance biosensing using silanized optical fibers. Sensors Actuators B Chem 216:518–526. https://doi.org/10.1016/j.snb.2015.04.069
27. Zhao J, Cao S, Liao C, Wang Y, Wang G, Xu X, Fu C, Xu G, Lian J, Wang Y (2016) Surface plasmon resonance refractive sensor based on silver-coated side-polished fiber. Sensors Actuators B Chem 230:206–211. https://doi.org/10.1016/j.snb.2016.02.020
28. Chang YF, Wang WH, Hong YW, Yuan RY, Chen KH, Huang YW, Lu PL, Chen YH, Chen YMA, Su LC, Wang SF (2018) Simple strategy for rapid and sensitive detection of avian influenza A H7N9 virus based on intensity-modulated SPR biosensor and new generated antibody. Anal Chem 90:1861–1869. https://doi.org/10.1021/acs.analchem.7b03934
29. Fen YW, Yunus WMM, Yusof NA (2012) Surface plasmon resonance optical sensor for detection of Pb 2 + based on immobilized p-tert-butylcalix [4] arene-tetrakis in chitosan thin film as an active layer. Sensors Actuators B Chem 171–172:287–293. https://doi.org/10.1016/j.snb.2012.03.070
30. Ali M, Karaaslan M, Sabah C (2018) Metamaterial-based fluid sensor for identifying different types of fuel oil samples, Chinese. J Phys 56:1872–1878. https://doi.org/10.1016/j.cjph.2018.08.018
31. Zubaidah S, Chao CC, Chau YC, Hanif A, Raziq M, Kooh R, Kumara NTRN, Chiang H (2021) Plasmonic refractive index sensor based on the combination of rectangular and circular resonators including baffles, Chinese. J Phys 71:286–299. https://doi.org/10.1016/j.cjph.2021.02.006
32. Horchani R (2018) Refractive index sensing using a linear graded plasmonic chain of metal nano-particles, Chinese. J Phys 56:1247–1251. https://doi.org/10.1016/j.cjph.2018.03.038
33. Haque T, Rouf HK (2021) DNA hybridization detection using graphene-MoSe2–Ag heterostructure-based surface plasmon resonance biosensor. Appl Phys A Mater Sci Process 127:1–13. https://doi.org/10.1007/s00339-021-04888-w
34. Islam MR, Iftekher ANM, Hasan KR, Nayen MJ, Bin Islam S, Islam R, Khan RL, Moazzam E, Tasnim Z (2021) Surface plasmon resonance based highly sensitive gold coated PCF biosensor. Appl Phys A Mater Sci Process 127:1–12. https://doi.org/10.1007/s00339-020-04162-5
35. Chung JW, Kim SD, Bernhardt R, Pyun JC (2005) Application of SPR biosensor for medical diagnostics of human hepatitis B virus (hHBV). Sensors Actuators, B Chem 111–112:416–422. https://doi.org/10.1016/j.snb.2005.03.055
36. Uzun L, Say R, Ünal S, Denizli A (2009) Production of surface plasmon resonance based assay kit for hepatitis diagnosis. Biosens Bioelectron 24:2878–2884. https://doi.org/10.1016/j.bios.2009.02.021
37. Uludag Y, Tothill IE (2012) Cancer biomarker detection in serum samples using surface plasmon resonance and quartz crystal microbalance sensors with nanoparticle signal amplification. Anal Chem 84:5898–904. https://doi.org/10.1021/ac300278p
38. Ertürk G, Özen H, Tümer MA, Mattiasson B, Denizli A (2016) Microcontact imprinting based surface plasmon resonance (SPR) biosensor for real-time and ultrasensitive detection of prostate specific antigen (PSA) from clinical samples. Sensors Actuators, B Chem 224:823–832. https://doi.org/10.1016/j.snb.2015.10.093
39. He L, Pagneux Q, Larroulet I, Serrano AY, Pesquera A, Zurutuza A, Mandler D, Boukherroub R, Szunerits S (2017) Label-free femtomolar cancer biomarker detection in human serum using graphene-coated surface plasmon resonance chips. Biosens Bioelectron 89:606–611. https://doi.org/10.1016/j.bios.2016.01.076
40. Liang RP, Yao GH, Fan LX, Qiu JD (2012) Magnetic Fe 3O 4@ Au composite-enhanced surface plasmon resonance for ultrasensitive detection of magnetic nanoparticle-enriched α-fetoprotein. Anal Chim Acta 737:22–28. https://doi.org/10.1016/j.aca.2012.05.043
41. Osman B, Uzun L, Beşirli N, Denizli A (2013) Microcontact imprinted surface plasmon resonance sensor for myoglobin detection. Mater Sci Eng C 33:3609–3614. https://doi.org/10.1016/j.msec.2013.04.041
42. Sener G, Uzun L, Say R, Denizli A (2011) Use of molecular imprinted nanoparticles as biorecognition element on surface plasmon resonance sensor. Sensors Actuators, B Chem 160:791–799. https://doi.org/10.1016/j.snb.2011.08.064
43. Bocková M, Chadtová Song X, Gedeonová E, Levová K, Kalousová M, Zima T, Homola J (2016) Surface plasmon resonance biosensor for detection of pregnancy associated plasma protein A2 in clinical samples. Anal Bioanal Chem 408:7265–7269. https://doi.org/10.1007/s00216-016-9664-z
44. Le Brun AP, Soliakov A, Shah DSH, Holt SA, McGill A, Lakey JH (2015) Engineered self-assembling monolayers for label free detection of influenza nucleoprotein. Biomed Microdevices 17:1–10. https://doi.org/10.1007/s10544-015-9951-z
45. Zeng C, Huang X, Xu J, Li G, Ma J, Ji HF, Zhu S, Chen H (2013) Rapid and sensitive detection of maize chlorotic mottle virus using surface plasmon resonance-based biosensor. Anal Biochem 440:18–22. https://doi.org/10.1016/j.ab.2013.04.026
46. Cairns TM, Ditto NT, Atanasiu D, Lou H, Brooks BD, Saw WT, Eisenberg RJ, Cohen GH (2019) Surface plasmon resonance reveals direct binding of herpes simplex virus glycoproteins gH/gL to gD and locates a gH/gL binding site on gD. J Virol 93:1–21. https://doi.org/10.1128/jvi.00289-19
47. Omidniaee A, Karimi S, Farmani A (2021) Surface plasmon resonance-based SiO2 Kretschmann configuration biosensor for the detection of blood glucose. Silicon. https://doi.org/10.1007/s12633-021-01081-9
48. Kamal Eddin FB, Fen YW, Omar NAS, Liew JYC, Daniyal WMEMM (2021) Femtomolar detection of dopamine using surface plasmon resonance sensor based on chitosan / graphene quantum dots thin film. Spectrochim Acta Part A Mol Biomol Spectrosc 120202. https://doi.org/10.1016/j.saa.2021.120202
49. Kamal Eddin FB, Fen YW (2020) Recent advances in electrochemical and optical sensing of dopamine. Sensors 20. https://doi.org/10.3390/s20041039
50. Kamal Eddin FB, Fen YW (2020) The principle of nanomaterials based surface plasmon resonance biosensors and its potential for dopamine detection. Molecules 25. https://doi.org/10.3390/molecules25122769
51. Omar NAS, Fen YW, Abdullah J, Mustapha Kamil Y, Daniyal WMEMM, Sadrolhosseini AR, Mahdi MA (2020) Sensitive detection of dengue virus type 2 E-proteins signals using self-assembled monolayers/reduced graphene oxide-PAMAM dendrimer thin film-SPR optical sensor. Sci Rep 10:1–15. https://doi.org/10.1038/s41598-020-59388-3
52. Omar NAS, Fen YW, Abdullah J, Zaid MHM, Daniyal WMEMM, Mahdi MA (2019) Sensitive surface plasmon resonance performance of cadmium sulfide quantum dots-amine functionalized graphene oxide based thin film towards dengue virus E-protein. Opt Laser Technol 114:204–208. https://doi.org/10.1016/j.optlastec.2019.01.038
53. Omar NAS, Fen YW (2017) Recent development of SPR spectroscopy as potential method for diagnosis of dengue virus E-protein. Sens Rev. SR-07–2017–0130. https://doi.org/10.1108/SR-07-2017-0130
54. Omar NAS, Fen YW, Saleviter S, Mohd W, Mustaqim E, Daniyal M, Ain N, Anas A (2019) Development of a graphene-based surface plasmon resonance optical sensor chip for potential biomedical application. https://doi.org/10.3390/ma12121928
55. Rosddi NNM, Fen YW, Omar NAS, Anas NAA, Hashim HS, Ramdzan NSM, Fauzi NIM, Anuar MF, Daniyal WMEMM (2021) Glucose detection by gold modified carboxyl-functionalized graphene quantum dots-based surface plasmon resonance. Optik 239:166779. https://doi.org/10.1016/j.ijleo.2021.166779

56. Situ C, Mooney MH, Elliott CT, Buijs J (2010) Advances in surface plasmon resonance biosensor technology towards high-throughput, food-safety analysis. TrAC-Trends Anal Chem 29:1305–1315. https://doi.org/10.1016/j.trac.2010.09.003
57. Zainuddin NH, Fen YW, Alwahib AA, Yaacob MH, Bidin N, Omar NAS, Mahdi MA (2018) Detection of adulterated honey by surface plasmon resonance optical sensor. Optik (Stuttg) 168:134–139. https://doi.org/10.1016/j.ijleo.2018.04.048
58. Fen YW, Yunus WMM, Talib ZA (2013) Analysis of Pb (II) ion sensing by crosslinked chitosan thin film using surface plasmon resonance spectroscopy. Opt-Int J Light Electron Opt 124:126–133. https://doi.org/10.1016/j.ijleo.2011.11.035
59. Daniyal WMEMM, Fen YW, Fauzi NIM, Hashim HS, Ramdzan NSM, Omar NAS (2020) Recent advances in surface plasmon resonance optical sensors for potential application in environmental monitoring. Sensors Mater 32:4191–4200
60. Ramdzan NSM, Fen YW, Anas NAA, Omar NAS, Saleviter S (2020) Development of biopolymer and conducting polymer-based optical sensors for heavy metal ion detection. Molecules 25:26
61. Hashim HS, Fen YW, Omar NAS, Abdullah J, Daniyal WMEMM, Saleviter S (2020) Detection of phenol by incorporation of gold modified-enzyme based graphene oxide thin film with surface plasmon resonance technique. Opt Express 28:9738
62. Fauzi NIM, YW Fen, Omar NAS, Saleviter S, Daniyal WMEMM, Hashim HS, Nasrullah M (2020) Nanostructured chitosan/maghemite composites thin film for potential optical detection of mercury ion by surface plasmon resonance investigation. Polymers 12:1497
63. Daniyal WMEMM, Fen YW, Abdullah J, Sadrolhosseini AR, Saleviter S, Omar NAS (2018) Exploration of surface plasmon resonance for sensing copper ion based on nanocrystalline cellulose-modified thin film. Opt Express 26:34880
64. Anas NAA, Fen YW, Omar NAS, Ramdzan NSM, Daniyal WMEMM, Saleviter S, Zainudin AA (2019) Optical properties of chitosan/hydroxyl-functionalized graphene quantum dots thin film for potential optical detection of ferric (III) ion. Opt Laser Technol 120:105724
65. Anas NAA, Fen YW, Omar NAS, Daniyal WMEMM, Ramdzan NSM, Saleviter S (2019) Development of graphene quantum dots-based optical sensor for toxic metal ion detection. Sensors 19:3850
66. Ramdzan NSM, Fen YW, Omar NAS, Anas NAA, Daniyal WMEMM, Saleviter S, Zainudin AA (2019) Optical and surface plasmon resonance sensing properties for chitosan/carboxyl-functionalized graphene quantum dots thin film. Optik 178:802–812
67. Fen YW, Yunus WMM (2013) Surface plasmon resonance spectroscopy as an alternative for sensing heavy metal ions: a review. Sens Rev 33:305–314
68. Daniyal WMEMM, Saleviter S, Fen YW (2018) Development of surface plasmon resonance spectroscopy for metal ion detection. Sens Mater 30:2023–2038
69. Zainudin AA, Fen YW, Yusof NA, Al-Rekabi SH, Mahdi MA, Omar NAS (2018) Incorporation of surface plasmon resonance with novel valinomycin doped chitosan-graphene oxide thin film for sensing potassium ion, Spectrochim. Acta A. Mol. Biomol. Spectrosc 191:111–115
70. Fen YW, Yunus WMM, Yusof NA, Ishak NS, Omar NAS, Zainudin AA (2015) Preparation, characterization and optical properties of ionophore doped chitosan biopolymer thin film and its potential application for sensing metal ion. Optik 126:4688–4692
71. Anas NAA, Fen YW, Yusof NA, Omar NAS, Daniyal WMEMM, Ramdzan NSM (2020) Highly sensitive surface plasmon resonance optical detection of ferric ion using CTAB/hydroxylated graphene quantum dots thin film. J Appl Phys 128:083105
72. Daniyal WMEMM, Fen YW, Abdullah J, Sadrolhosseini AR, Saleviter S, Omar NAS (2019) Label-free optical spectroscopy for characterizing binding properties of highly sensitive nanocrystalline cellulose-graphene oxide based nanocomposite towards nickel ion. Spectrochim Acta A Mol Biomol Spectrosc 212:25–31
73. Saleviter S, Fen YW, Daniyal WMEMM, Abdullah J, Sadrolhosseini AR, Omar NAS (2019) Design and analysis of surface plasmon resonance optical sensor for determining cobalt ion based on chitosan-graphene oxide decorated quantum dots-modified gold active layer. Opt Express 27:32294–32307
74. Hashim HS, Fen YW, Omar NAS, Fauzi NIM, Daniyal WMEMM (2021) Recent advances of priority phenolic compounds detection using phenol oxidases-based electrochemical and optical sensors. Measurement 184:109855. https://doi.org/10.1016/j.measurement.2021.109855
75. Wei W, Nong J, Zhu Y, Zhang G, Wang N, Luo S, Chen N, Lan G, Chuang CJ, Huang Y (2018) Graphene/Au-enhanced plastic clad silica fiber optic surface plasmon resonance sensor. Plasmonics 13:1–9. https://doi.org/10.1007/s11468-017-0534-0
76. Arumugasamy SK, Govindaraju S, Yun K (2020) Electrochemical sensor for detecting dopamine using graphene quantum dots incorporated with multiwall carbon nanotubes. Appl Surf Sci 508:145294. https://doi.org/10.1016/j.apsusc.2020.145294
77. Ben Aoun S (2017) Subject Category : Subject Areas : Author for correspondence : Nanostructured carbon electrode modified with N-doped graphene quantum dots – chitosan nanocomposite : a sensitive electrochemical dopamine sensor. R Soc Open Sci 4:1–12
78. Weng S, Liang D, Qiu H, Liu Z, Lin Z, Zheng Z, Liu A, Chen W, Lin X (2015) Sensors and Actuators B : Chemical A unique turn-off fluorescent strategy for sensing dopamine based on formed polydopamine (pDA) using graphene quantum dots (GQDs) as fluorescent probe. Sensors Actuators B Chem 221:7–14. https://doi.org/10.1016/j.snb.2015.06.093
79. Zhou X, Ma P, Wang A, Yu C, Qian T, Wu S, Shen J (2014) Dopamine fluorescent sensors based on polypyrrole/graphene quantum dots core/shell hybrids. Biosens Bioelectron 64:404–410. https://doi.org/10.1016/j.bios.2014.09.038
80. Yan Y, Liu Q, Du X, Qian J, Mao H, Wang K (2015) Visible light photoelectrochemical sensor for ultrasensitive determination of dopamine based on synergistic effect of graphene quantum dots and TiO2 nanoparticles. Anal Chim Acta 853:258–264. https://doi.org/10.1016/j.aca.2014.10.021
81. Fen YW, Yunus WMM (2013) Utilization of chitosan-based sensor thin films for the detection of lead ion by surface plasmon resonance optical sensor. IEEE Sens J 13:1413–1418
82. Fen YW, Yunus WMM, Yusof NA (2011) Optical properties of cross-linked chitosan thin film for copper ion detection using surface plasmon resonance technique. Opt Appl 41:999–1013
83. Fen YW, Yunus WMM, Moksin MM, Talib ZA, Yusof NA (2011) Surface plasmon resonance optical sensor for mercury ion detection by crosslinked chitosan thin film. J Optoelectron Adv Mater 13:279–285
84. Fen YW, Yunus WMM, Talib ZA (2013) Analysis of Pb(II) ion sensing by crosslinked chitosan thin film using surface plasmon resonance spectroscopy. Opt-Int J Light Electron Opt 124:126–133. https://doi.org/10.1016/j.ijleo.2011.11.035
85. Bahrami A, Sadrolhosseini AR, Mamdoohi G, Bahzad K, Abdi MM (2015) Surface plasmon sensor based on polypyrrole multiwalled carbon nanotube composite layer to detect Al (III) in aqueous solution. Dig J Nanomater Biostructures 10:535–541
86. Schasfoort RBM (2017) Handbook of surface plasmon resonance. Royal Society of Chemistry
87. Homola J (2006) Electromagnetic theory of surface plasmons. Springer Ser Chem Sens Biosens 3–44. https://doi.org/10.1007/5346_013

88. Bashkatov AN, Genina EA (2003) Water refractive index in dependence on temperature and wavelength: a simple approximation. Opt Technol Biophys Med IV 5068:393–395
89. Franca AS, Nollet LML (eds) (2017) Spectroscopic methods in food analysis (1st ed). CRC Press. https://doi.org/10.1201/9781315152769
90. Fernandes SC, Vieira IC, Peralta RA, Neves A (2010) Development of a biomimetic chitosan film-coated gold electrode for determination of dopamine in the presence of ascorbic acid and uric acid. Electrochim Acta 55:7152–7157. https://doi.org/10.1016/j.electacta.2010.06.062
91. Shalabney A, Abdulhalim I (2011) Sensitivity-enhancement methods for surface plasmon sensors. Laser Photonics Rev 5:571–606. https://doi.org/10.1002/lpor.201000009
92. Fouad S, Sabri N, Jamal ZAZ, Poopalan P (2017) Surface plasmon resonance sensor sensitivity enhancement using gold-dielectric material. Int J Nanoelectron Mater 10:147–156
93. Daniyal WMEMM, Fen YW, Abdullah J, Sadrolhosseini AR, Mahdi MA (2021) Design and optimization of surface plasmon resonance spectroscopy for optical constant characterization and potential sensing application: theoretical and experimental approaches. Photonics 8:361
94. Usman F, Dennis JO, Seong KC, Ahmed AY, Ferrell TL, Fen YW, Sadrolhosseini AR, Ayodele OB, Meriaudeau F, Saidu A (2019) Enhanced sensitivity of surface plasmon resonance biosensor functionalized with doped polyaniline composites for the detection of low-concentration acetone vapour. J Sensors 2019. https://doi.org/10.1155/2019/5786105
95. Mudgal N, Saharia A, Agarwal A, Singh G (2020) ZnO and Bi-metallic (Ag–Au) layers-based surface plasmon resonance (SPR) biosensor with $BaTiO_3$ and graphene for biosensing applications. IETE J Res 1:1–8. https://doi.org/10.1080/03772063.2020.1844074